Journal of Power Sources 233 (2013) 47–61

Contents lists available at SciVerse ScienceDirect

Journal of Power Sources

journal homepage: www.elsevier.com/locate/jpowsour

Numerical and analytical modeling of lithium ion battery thermal behaviors with different cooling designs

Jingzhi Xun, Rui Liu, Kui Jiao*

State Key Laboratory of Engines, Tianjin University, 92 Weijin Rd, Tianjin 300072, China

HIGHLIGHTS

- ► Numerical and analytical models are developed for thermal management of Li battery.
- ► Same cooling channel to battery volume ratio leads to same average temperature.
- ► Larger channel improves evenness of temperature distribution and energy efficiency.

ARTICLE INFO

Article history:
Received 30 September 2012
Received in revised form
2 December 2012
Accepted 17 January 2013
Available online 31 January 2013

Keywords:
Thermal management
Lithium ion battery stack
Discharging process
Cooling channel
Temperature distribution

ABSTRACT

Thermal management is critically important to maintain the performance of lithium ion battery stacks. In this study, a numerical model and an analytical model for the thermal management of lithium ion battery stacks are developed to investigate the thermal behaviors of flat-plate and cylindrical stacks during discharging processes. It is found that for the same volume ratio of cooling channel and battery of flat-plate design, changing the channel size and the number of channels results in similar average battery temperatures, however, increasing the channel size improves the cooling energy efficiency but leads to more unevenly distributed temperature, and vice versa. The volume ratio of cooling channel to battery needs to be higher than 0.014 for flat-plate design when the Reynolds number of cooling air is around 2000 or higher with a high discharging rate of 2 C. The cylindrical battery stacks considered in this study are generally less compact and more energy-efficient in cooling than the flat-plate battery stacks, and the general thermal behaviors are similar between these two designs. A counter-flow arrangement of the cooling channels or changing the flow direction of the co-flow arrangement periodically may also help the thermal management.

1. Introduction

Air pollution and greenhouse effect, with a large part contributed by the emissions from vehicles, has become a global environmental problem and received great attention in many countries. To decrease the amount of pollutant and greenhouse gas, governments from different countries have formulated various kinds of emission regulations. Electric and hybrid electric vehicles are promising solutions to meet these increasingly stringent emission regulations and the ever growing demand for vehicles. Therefore, for automotive applications, a large demand for rechargeable batteries with high energy and power densities, long lifetime and safe operation has been created.

Among the different kinds of rechargeable batteries, lithium ion battery is relatively a suitable choice for electric and hybrid electric vehicles, due to its advantages in energy and power densities, durability and safety by comparing with other kinds of rechargeable batteries [1]. In order to supply the power required, single lithium ion batteries often need to be connected in series to form battery stacks [2], and the battery stacks for automotive applications need to work under the conditions with high discharging and charging rates, which may lead to high heat generation rates inside the stacks, potentially lowering the performance and causing safety problems [3]. Moreover, a battery stack usually has a cut off state of charge (SOC) to protect it from over depletion [3]. For a battery stack operating in a discharging process, the temperature is often unevenly distributed, and the cut off SOC often needs to be set to ensure the safety of the battery unit with the highest temperature, leading to unused or wasted energy in other battery units. In addition to the safety and durability issues caused by the overheating problem, a low temperature can also decrease the battery

* Corresponding author. Tel.: +86 22 87455090; fax: +86 22 27406949.
E-mail address: kjiao@tju.edu.cn (K. Jiao).

0378-7753/$ – see front matter © 2013 Elsevier B.V. All rights reserved.
http://dx.doi.org/10.1016/j.jpowsour.2013.01.095

Nomenclature

A_c	cross-sectional area of cooling channel (m^2)
c_{pa}	Heat capacity of air (J kg^{-1} °C^{-1})
c_{pb}	heat capacity of the battery units (J kg^{-1} °C^{-1})
C	charge capacity (A h)
E_{oc}	open circuit voltage of the battery (V)
F	Faraday's constant 96,458 (C mol^{-1})
h	convective heat transfer coefficient (W m^{-2} °C)
i	current density (A m^{-3})
I	discharge current (A)
k_a	thermal conductivity of air (W m^{-1} °C^{-1})
k_b	thermal conductivity of the battery units (W m^{-1} °C^{-1})
L	length of cooling channel (m)
N	number of electrons participation in the reaction
Nu	Nusselt number
P_c	power loss of air flow in cooling channel (W)
R	internal resistance (Ω m^{-3})
Re	Reynolds number
S	entropy (J mol^{-1} K^{-1})
S_{ab}	heat absorption rate by battery per unit volume (W m^{-3})
S_T	heat generation rate per unit volume (W m^{-3})
SOC	state of charge
t	time (s)
T_a	temperature of air (°C)
T_b	temperature of the battery units (°C)
v	velocity of air flow (m s^{-1})
V	voltage, V
x	spatial coordinate (m)
y	spatial coordinate (m)
z	spatial coordinate (m)

Greek letters

α	volume ratio between cooling channel and battery
β	ratio between heat taken by the cooling fluid and power consumption of compressor
ρ_a	air density (kg m^{-3})
ρ_b	battery average density (kg m^{-3})
Λ	volume of battery unit (m^3)

Subscripts/superscripts

a	air
b	battery
Inlet	velocity inlet of the cooling channel
Outlet	pressure outlet of the cooling channel

capacities [4]. All these features require the temperature in a battery stack to be kept in certain ranges and the temperature variation needs to be minimized. Therefore, thermal management is significantly important for lithium ion battery stacks in the automotive and other applications requiring high discharging and charging rates.

Both the empirical models utilizing experimental data [5–11] and numerical models derived from the first principles of mass and heat transfer and battery electrochemistry [12–16] were developed for lithium ion battery thermal management. For the empirical models, Smith et al. [5] developed an electrical-thermal coupled model of a lithium ion cell and a module with 16 cells in parallel. Equivalent electrical and thermal circuits were integrated into their model, and the modeling results were used to assess the battery thermal safety margin. Forgeza et al. [6] developed a lumped thermal model of a cylindrical $LiFePO_4$/graphite lithium ion battery, and the heat transfer coefficients, heat capacity and thermal resistance used in this model were obtained experimentally. This model was then used to obtain the internal temperature based on the measured current and voltage. Maleki and Shanmsuri [7] investigated the thermal behavior of a lithium ion battery under various working conditions, and it was found that the heat generations from the battery and the control device are all significant. Al-Hallaj et al. [8] developed an electrochemical-calorimetric method to study the thermal behavior of commercial lithium ion batteries. The amount of heat generation was measured based on the SOC at the end of the discharging processes for this method. Mills and Al-Hallaj [9] designed and modeled a passive thermal management system with an impregnated phase change material (PCM) for a lithium ion battery stack. Kizilel et al. [10] and Duan and Naterer [11] also studied the thermal behavior of the battery stacks with PCM cooling system under various conditions.

Numerical models for the thermal management of lithium ion batteries were also developed in previous studies. Karimi and Li [12] simulated the effect of cooling condition and stack configuration on the temperature distribution, and found that a cooling strategy based on distributed forced convection is an efficient and cost-effective method. Chen and Evans [13] developed a two-dimensional model of lithium ion batteries, and investigated the effect of component property, stack size and cooling condition on the performance, some methods to maintain the operating temperature were also proposed. Inui et al. [14] developed two- and three-dimensional models of lithium ion batteries to simulate the transient temperature distribution, and found that the battery with laminated cross section performed better than the one with square cross section in preventing the temperature increment. Fang et al. [15] used an electrochemical-thermal coupled method to study the behavior of a lithium ion battery at different temperatures. Sabbah et al. [16] and Kizilel et al. [17] compared the effectiveness of active cooling (e.g. forced convection) and passive cooling (e.g. PCM) for the thermal management of battery stacks.

By reviewing the previous thermal management studies for lithium ion batteries, it is found that most of them focused on single or a number of battery units under certain discharging or charging rates. The effect of cooling channel design on the thermal behavior of lithium ion battery stacks still need to be investigated in details. For battery stacks, the size and number of cooling channels are the key parameters determining the effectiveness of thermal management, and a parameter can be defined as

$$\alpha = \frac{\text{volume of cooling channel}}{\text{volume of battery unit}} \quad (1)$$

Table 1
Geometric parameters and configurations of the different layers in a single battery cell [1].

Layer	Thickness (μm)
Graphite	120
Copper	20
Graphite	120
Electrolyte	40
$LiCoO_2$	180
Aluminum	20
$LiCoO_2$	180
Separator	50
Total thickness of a single cell	730

Table 2
Properties of the different materials in a battery cell [1].

Material	Thermal conductivity ($W\ m^{-1}\ ^{\circ}C^{-1}$)	Density ($kg\ m^{-3}$)	Specific heat capacity ($J\ kg^{-1}\ ^{\circ}C^{-1}$)
Copper	398	8930	386
Graphite	1.04	1347	1437
Electrolyte	0.59	1375	1375
$LiCoO_2$	4	715	715
Aluminum	237	902	902
Separator	0.35	1552	1552

where α represents the compactness of a battery stack, and a smaller α corresponds to a more compact design. The ratio between the heat removal rate by the cooling fluid from a battery stack and the cooling power consumption is another key parameter, can be considered as the cooling efficiency factor:

$$\beta = \frac{\text{heat taken by cooling air}}{\text{power consumption for supplying cooling air}} \quad (2)$$

and a larger β corresponds to a higher energy efficiency. For lithium ion batteries in automotive applications, both the compactness (α) and energy efficiency (β) are critical parameters due to the high requirements of energy and power densities. The cooling channel design directly affects these two parameters, and simultaneously reducing the cooling channel size and number and enhancing the cooling effect and efficiency are of significant importance.

In this study, a multi-dimensional numerical model and an analytical model for the thermal management of lithium ion battery stacks are developed. The effect of cooling channel design on the thermal behavior of lithium ion battery stacks during discharging processes is investigated comprehensively. The two critical parameters representing the compactness (α) and energy efficiency (β) are analyzed based on the simulation results.

2. Numerical model

2.1. Physical problem

The battery stacks used for electric and hybrid electric vehicles include many battery units connected in series or parallel; each battery unit is formed by a number of cells often linked in series; and each single cell has different layers including two thin layers of graphite mounted on a copper foil, two layers of $LiCoO_2$ mounted on an aluminum foil, an electrolyte layer between the electrodes, and a separator between the neighboring cells. The thicknesses, configurations and thermal–physical properties of these layers are shown in Tables 1 and 2. The electrochemical reactions are

$$\text{Anode}: \quad LiC_6 \Leftrightarrow C_6 + Li^+ + e^- \quad (3)$$

$$\text{Cathode}: \quad CoO_2 + Li^+ + e^- \Leftrightarrow LiCoO_2 \quad (4)$$

$$\text{Overall}: \quad CoO_2 + LiC_6 \Leftrightarrow LiCoO_2 + C_6 \quad (5)$$

The electrochemical reactions occur from the left to right side of Equations (3)–(5) during a discharging process, and vice versa.

The two common designs of lithium ion batteries are flat-plate and cylindrical, which are all considered in this study. The schematics of the flat-plate and cylindrical designs are shown in Figs. 1 and 2, respectively. In the flat-plate design (Fig. 1), the battery stack includes a number of battery units, and the cooling channels are distributed between the battery units. In the cylindrical design

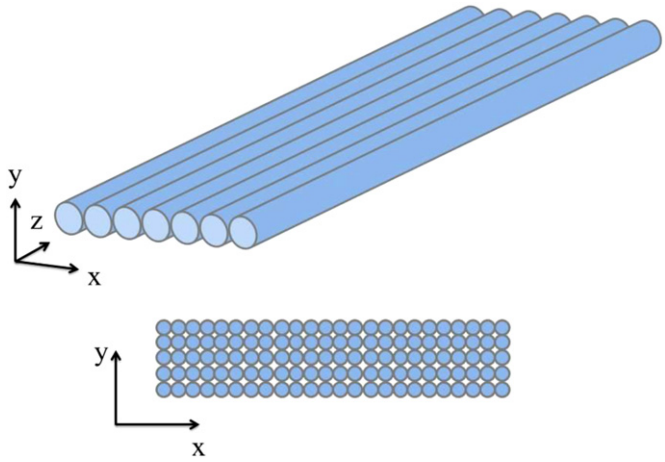

Fig. 2. Schematic of a cylindrical lithium ion battery stack.

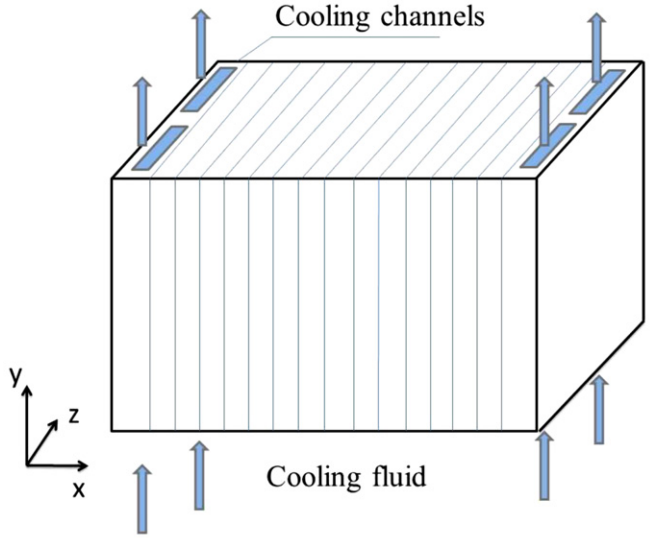

Fig. 1. Schematic of a flat-plate lithium ion battery stack.

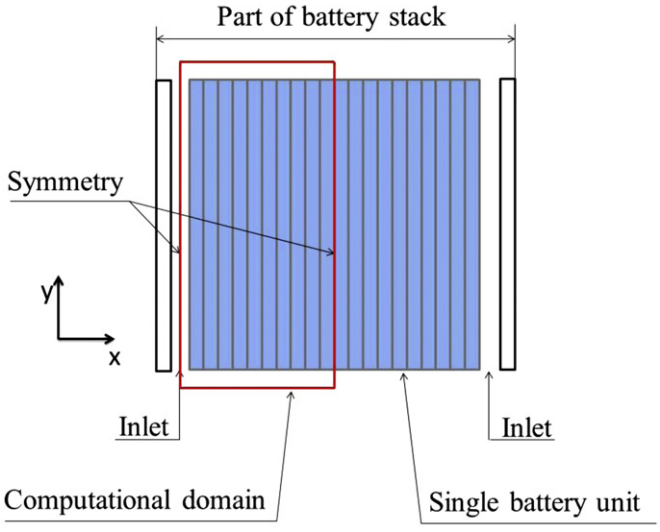

Fig. 3. Simplification of the computational domain for a flat-plate battery stack.

Table 3
Configurations of the flat-plate and cylindrical battery stacks.

	Battery unit number	Cell number in each unit	Thickness of the channel (mm)	Channel length (mm)	α
Flat-plate battery	20	10	2	250	0.014
			4		0.027
			8		0.055
			12		0.082
	10		4		0.055
	20				0.027
	30				0.018
	Battery unit diameter (mm)		Distance between units (mm)	Channel length (mm)	α
Cylindrical battery	18		0	650	0.33
			1		0.57
			2		0.90
			3		1.26
			6		2.54

(Fig. 2), the battery includes a number of cylindrical battery units, and the space among the battery units forms the cooling channels.

For the flat-plate design in Fig. 1, with coolant flow along the *y*-direction and large channel size along the *z*-direction, the flat-plate stack can be represented by a two-dimensional computational domain, as shown in Fig. 3, with two symmetry boundaries on the two sides of the *x*-direction, representing the repeating units in the stack. The flat-plate and cylindrical cooling channel designs for the simulations are shown in Table 3. The cooling channel sizes along the *x*-direction considered in this study are 2, 4, 8 and 12 mm with 20 battery units between two cooling channels; and with a channel size of 4 mm, the number of battery units between two cooling channels are 10, 20 and 30. The length of the cooling channels in the flat-plate design is 250 mm. In addition, each battery unit includes 10 cells.

For the cylindrical design in Fig. 2, the stack can be represented by a quarter of a battery unit, as shown in Fig. 4, with symmetry boundaries on the four sides, representing the repeating units in the stack. In this study, the cross-sectional area (diameter) of the cylindrical battery unit is a constant, and the cooling channel sizes are changed according to the distances between the cylindrical battery units, as given in Table 3. The length of the cooling channels in the cylindrical design is 650 mm. The corresponding computational domains and meshes for the flat-plate and cylindrical designs are shown in Figs. 5 and 6, which are two- and three-dimensional, respectively.

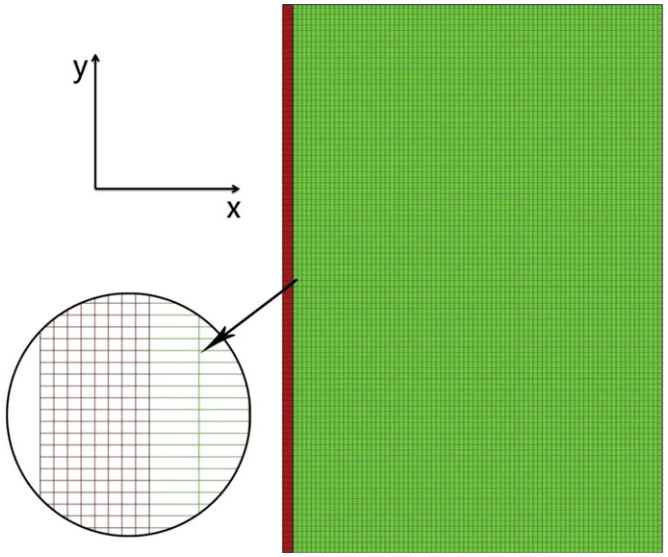

Fig. 5. Computational domain and mesh of a flat-plate battery stack (2× minification along the *y*-direction).

Because the cooling channels have the same length (along the flow direction) as the battery units, the volume ratio of cooling channels and battery units defined in Equation (1) is also equal to the ratio of the cross-sectional areas. The cooling fluid is considered to be air, because it was reported to be sufficient for the cooling requirement of lithium ion battery stacks [12], and the design and operating requirements are simple. The properties of air are shown in Table 4.

For the flat-plate design, the number of battery units in a stack and the width of the cooling channel are the two important parameters to be investigated. For the cylindrical design, the

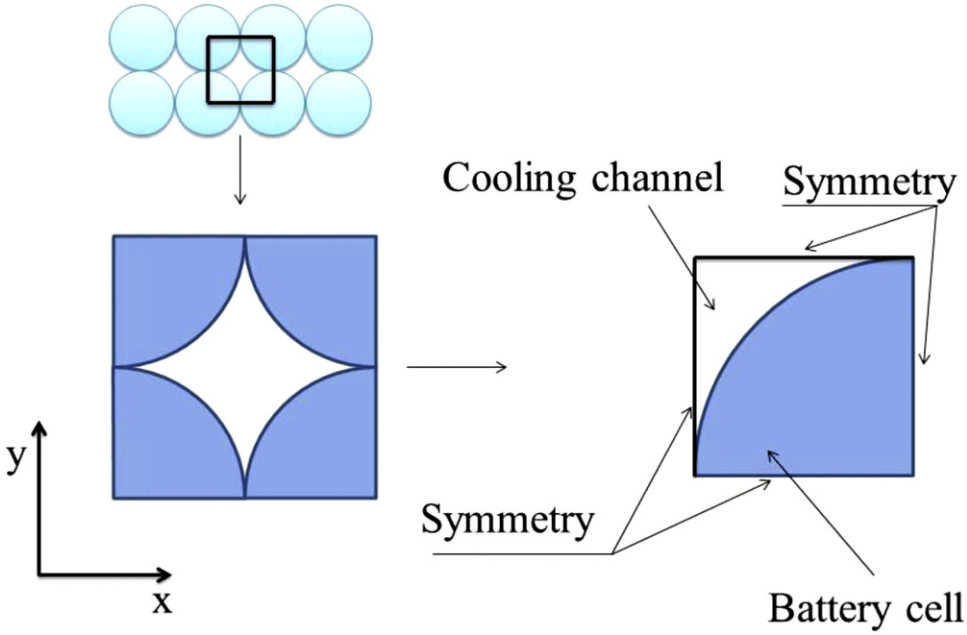

Fig. 4. Simplification of the computational domain for a cylindrical battery stack.

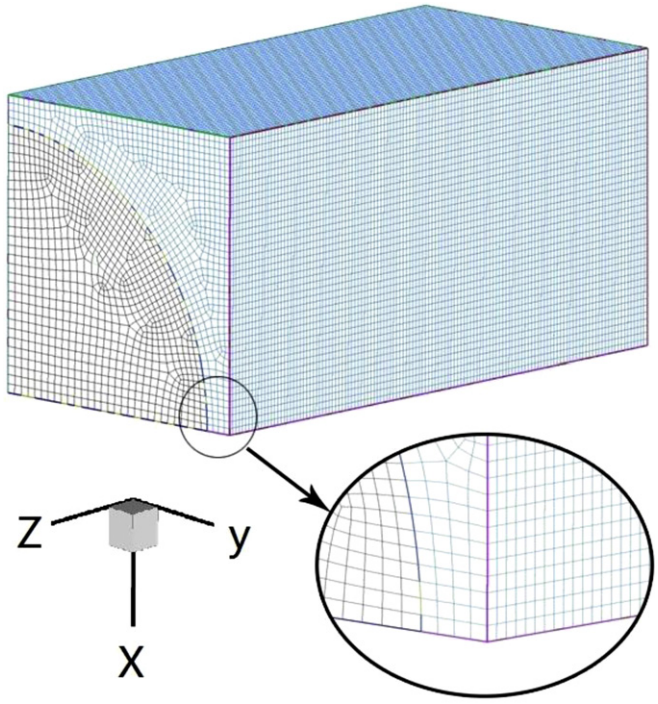

Fig. 6. Computational domain and mesh of a cylindrical battery stack (32.5× minification along the *z*-direction).

parameter to be investigated is the size of the cooling channel, determined by the distances between the cylindrical battery units. The effect of inlet Reynolds number of the cooling air is also investigated. The operating conditions are given in Table 5. In addition, the allowed operating temperature range for the battery is from 0 °C to 65 °C [18].

2.2. Assumptions

The cooling air flow is assumed to be incompressible and laminar due to the low flow velocity and short characteristic lengths considered in this study (Reynolds number < 2300). Even though the individual layers in a cell have different electrical resistances, the thicknesses (on the level of μm) of these layers are negligible by comparing with the size of the stacks. Therefore, the equivalent internal resistance [14] of each cell is used. Moreover, because of the negligible thicknesses of the different layers in each cell, the heat generation due to entropy change is assumed to be uniformly distributed in each cell.

2.3. Conservation equations

The mass conservation equation of the air in cooling channel is

$$\frac{\partial \rho_a}{\partial t} + \nabla\cdot(\rho_a \vec{v}) = 0 \tag{6}$$

where ρ_a (kg m^{-3}) is the density of air, $\vec{v}$ (m s^{-1}) is the velocity vector of air. The momentum conservation equation of air is

Table 4
Properties of air.

Density	1.225 (kg m^{-3})
Specific heat capacity	1006.43 (J kg^{-1} °C^{-1})
Thermal conductivity	0.0242 (W m^{-1} °C^{-1})
Viscosity	1.7894 × 10^{-5} (kg m^{-1} s^{-1})

Table 5
Operating conditions.

Initial temperature	20 (°C)
Capacity of the battery stack	20 (A h)
Discharging rate	2 C
Inlet Reynolds number of cooling air	230, 460, 690, 920, 1150, 1380, 1610, 1840, 2070, 2300

$$\frac{\partial}{\partial t}(\rho_a \vec{v}) + \nabla\cdot(\rho_a \vec{v}\vec{v}) = -\nabla p \tag{7}$$

where p (Pa) is the static pressure. The energy conservation equation of air is

$$\frac{\partial}{\partial t}(\rho_a c_{pa} T_a) + \nabla\cdot(\rho_a c_{pa} \vec{v} T_a) = \nabla\cdot(k_a \nabla T_a) \tag{8}$$

where T_a (°C) is the temperature of air, k_a (W m^{-1} °C^{-1}) is the thermal conductivity of air, and c_{pa} (J kg^{-1} °C^{-1}) is the specific heat capacity of air. The energy conservation equation of the battery units is

$$\frac{\partial}{\partial t}\left(\rho_b c_{pb} T_b\right) = \nabla\cdot(k_b \nabla T_b) + S_T \tag{9}$$

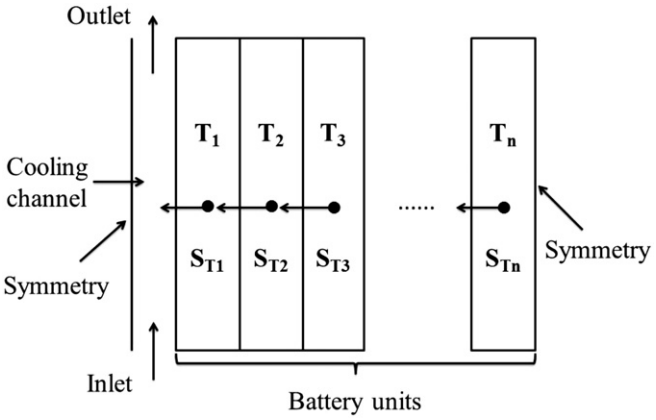

Fig. 7. Schematic of the analytical model for a flat-plate battery stack.

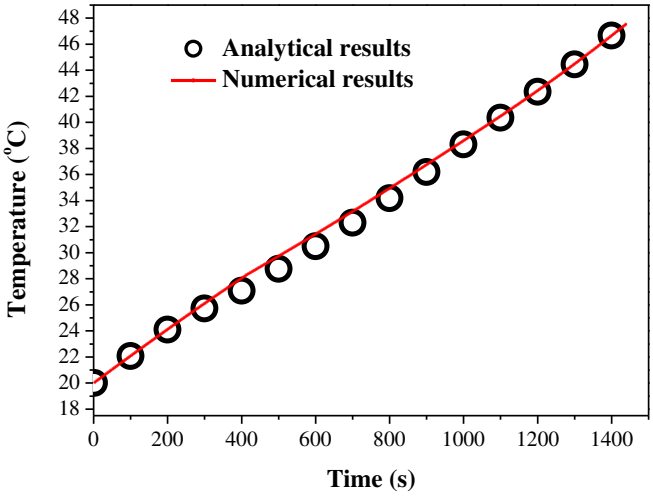

Fig. 8. Comparison between numerical and analytical results for the evolution of volume averaged temperature of a flat-plate battery stack during a discharging process.

where ρ_b (kg m^{-3}) is the density of battery materials, T_b (°C) is the temperature in battery units, k_a (W m^{-1} °C^{-1}) is the thermal conductivity of battery materials, and c_{pb} (J kg^{-1} °C^{-1}) is the heat capacity of battery materials. The source term, S_T (W m^{-3}), represents the total heat generation rate:

$$S_T = I(E_{oc} - V) + IT_b\frac{dE_{oc}}{dT_b} \quad (10)$$

where I (A) is the discharging current, E_{oc} (V) is the open circuit voltage, V (V) is the operating voltage. This equation can also be written as [14]

$$S_T = i^2R - T_b\Delta S\frac{i}{nF} \quad (11)$$

where i (A m^{-3}) is the discharging current per unit volume and n is the number of electrons participating in the reaction, F (96485 C mol^{-1}) is Faraday's constant, ΔS (J mol^{-1} K^{-1}) is the entropy change, and R (Ω m^{-3}) is the equivalent internal resistance, which is the summation of the ohmic and reaction resistances [14]. Therefore, the first term on the right hand side of Equation (11) represents the ohmic and reaction heat generations, and the second term represents the heat generation due to the entropy change. The measured equivalent internal resistance (R, Ω m^{-3}) for the SONY-US18650 as a function of SOC and temperature (T, °C) is used [14]:

$$\begin{aligned} R &= 2.258\times10^{-6}\mathrm{SOC}^{-0.3952} \quad T = 20^\circ\mathrm{C} \\ R &= 1.857\times10^{-6}\mathrm{SOC}^{-0.2787} \quad T = 30^\circ\mathrm{C} \\ R &= 1.659\times10^{-6}\mathrm{SOC}^{-0.1692} \quad T = 40^\circ\mathrm{C} \end{aligned} \quad (12)$$

The entropy change, ΔS (J mol^{-1} K^{-1}), can be calculated as [12]

$$\begin{aligned} \Delta S &= 99.88\mathrm{SOC} - 76.67 \quad 0 \le \mathrm{SOC} \le 0.77 \\ \Delta S &= 30 \quad 0.77 \le \mathrm{SOC} \le 0.87 \\ \Delta S &= -20 \quad 0.87 \le \mathrm{SOC} \le 1 \end{aligned} \quad (13)$$

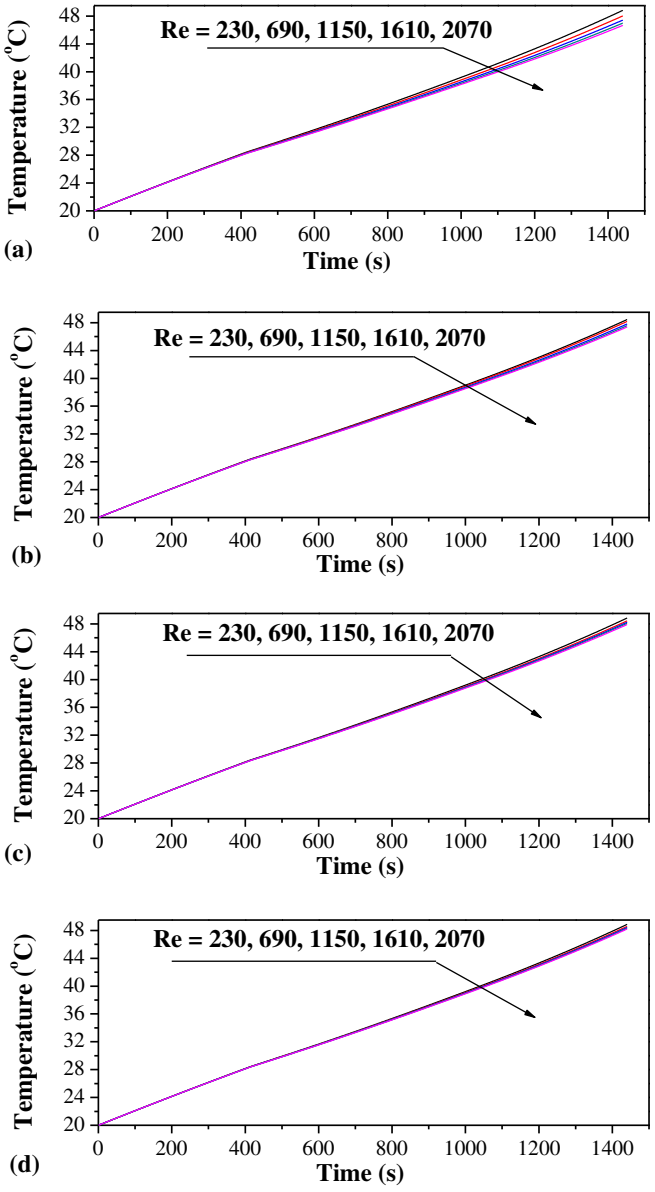

Fig. 9. Evolutions of volume averaged temperatures of the flat-plate battery with different cooling channel sizes and inlet Reynolds numbers of cooling air during the discharging processes. (a) channel size = 2 mm, α = 0.014; (b) channel size = 4 mm, α = 0.027; (c) channel size = 8 mm, α = 0.055; (d) channel size = 12 mm, α = 0.082.

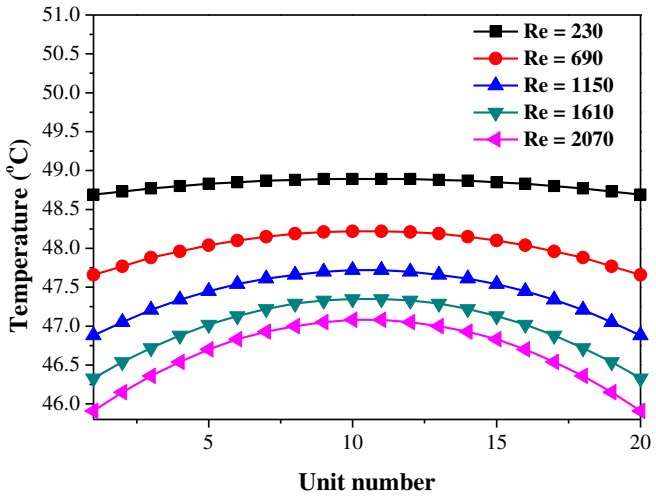

Fig. 10. Volume averaged temperature in each unit of the flat-plate battery stack with a cooling channel size of 4 mm (α = 0.027) and different inlet Reynolds numbers of cooling air at the end of the discharging processes.

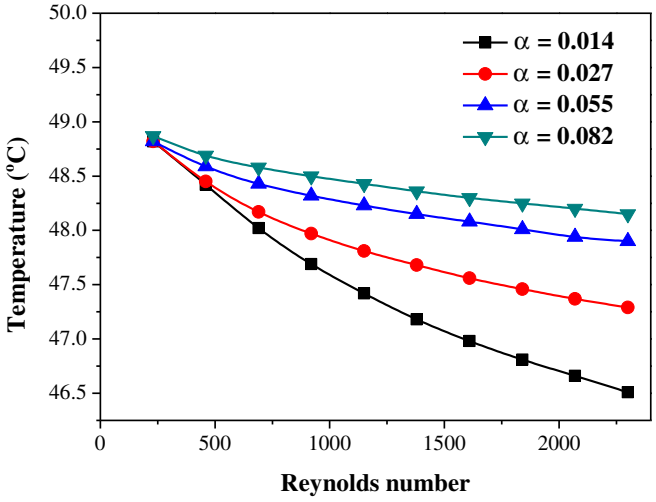

Fig. 11. Volume averaged temperatures of the flat-plate battery with different inlet Reynolds numbers of cooling air and cooling channel sizes at the end of the discharging processes (channel size = 2 mm, α = 0.014; channel size = 4 mm, α = 0.027; channel size = 8 mm, α = 0.055; channel size = 12 mm, α = 0.082).

where SOC can be determined as

$$\mathrm{SOC} = 1 - \frac{it}{C} \tag{14}$$

In a discharging process, the voltage is defined as

$$V = E_{oc} - IR \tag{15}$$

The heat absorption rate by the battery per unit volume (S_{ab}, W m^{-3}) is

$$S_{ab} = \rho_b c_{pb} \frac{\partial T_b}{\partial t} \tag{16}$$

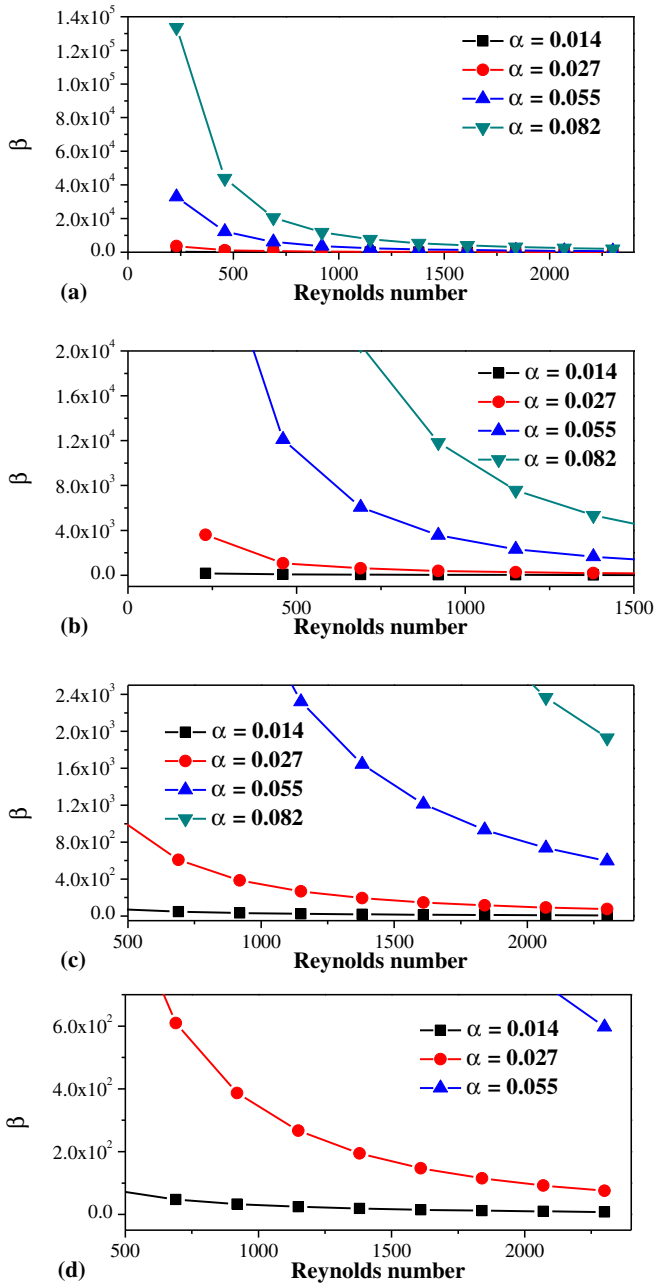

Fig. 12. Cooling efficiency factors (β) of the flat-plate battery stacks with different channel sizes (α) and inlet Reynolds numbers of cooling air for the discharging processes (channel size = 2 mm, α = 0.014; channel size = 4 mm, α = 0.027; channel size = 8 mm, α = 0.055; channel size = 12 mm, α = 0.082).

The power loss of the air flow (P_c, W) through the cooling channel is

$$P_c = p_{drop} A_c v \tag{17}$$

where p_{drop} (Pa) is the pressure drop of air through the channel, A_c (m^2) is the cross-sectional area of the cooling channel, and v (m s^{-1}) is the air flow velocity along the channel. For calculating the cooling efficiency factor, β (Equation (2)), the heat removal rate from the battery can be represented by the difference between the heat generation rate (Equation (11)) and heat absorption rate (Equation (16)), and by neglecting the power loss in the compressor or blower to supply cooling air, β can be represented as

$$\beta = \frac{(S_T - S_{ab})\Lambda}{P_c} \tag{18}$$

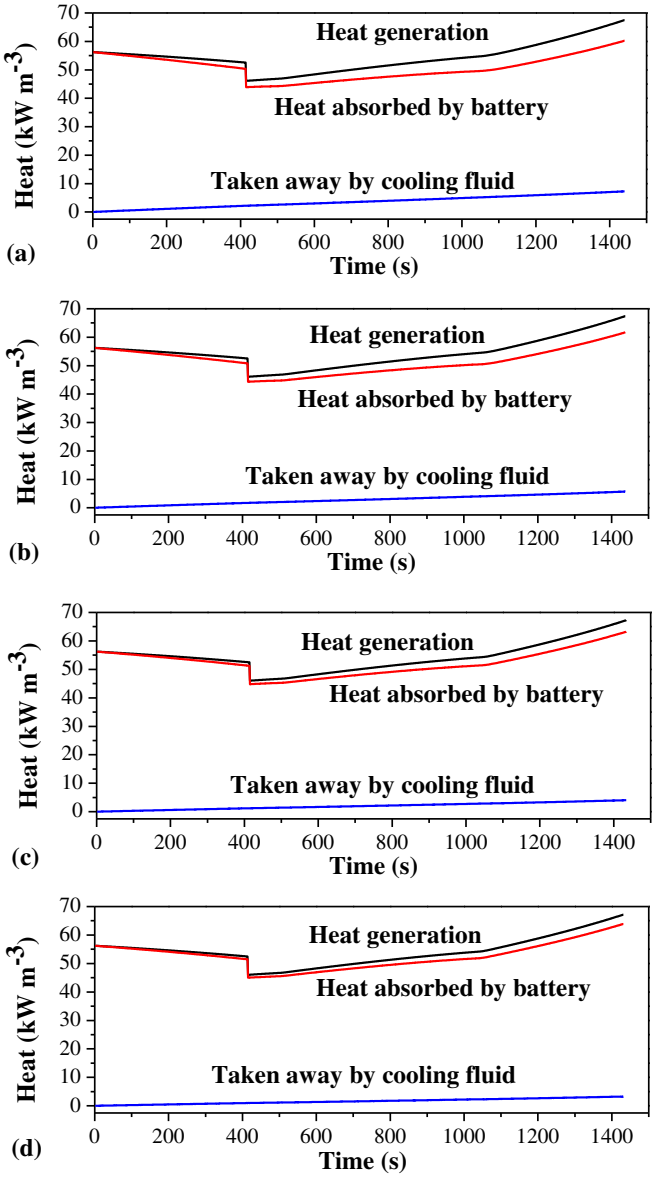

Fig. 13. Rates of heat generation, heat absorbed by battery and heat taken away by cooling air for the flat-plate battery stacks with an inlet Reynolds number of 1150 and different cooling channel sizes during the discharging processes. (a) channel size = 2 mm, α = 0.014; (b) channel size = 4 mm, α = 0.027; (c) channel size = 8 mm, α = 0.055; (d) channel size = 12 mm, α = 0.082.

where Λ (m^3) is the volume of battery. It should be noticed that if the power loss in the air compressor or blower is considered, the value of β should be higher than in Equation (18).

2.4. Initial and boundary conditions

All the simulations start from a room temperature, 20 °C. Velocity is defined for the inlet of cooling channel, and the inlet temperature is also defined at 20 °C. Atmospheric pressure is defined at the cooling channel outlet. By defining the air flow velocity at the cooing channel inlet, the Reynolds number in the cooling channel can also be indicated. Therefore, the effect of Reynolds number on the thermal behavior of battery can be investigated by using this numerical model. Since only laminar flow is considered in this study (laminar flow could be sufficient for battery cooling with proper design [12]), ten different Reynolds numbers from 230 to 2300 (in laminar flow region) are defined to comprehensively investigate the Reynolds number effect. At the ends of the flat-plate (*y*-direction, Fig. 5) and cylindrical (*z*-direction, Fig. 6) battery units, heat insulation boundary conditions are defined (the heat flux is 0). This boundary condition is reasonable because the battery units need to be covered by other materials for protection, resulting in considerable thermal resistances. In fact, the same heat insulation boundary condition was also used in previous modeling studies (e.g. Ref. [12]). In addition, symmetry boundary conditions are also defined as introduced before with Figs. 3 and 4.

2.5. Numerical procedures

This numerical model is implemented in a computational fluid dynamics software package, Fluent, with its user defined functions

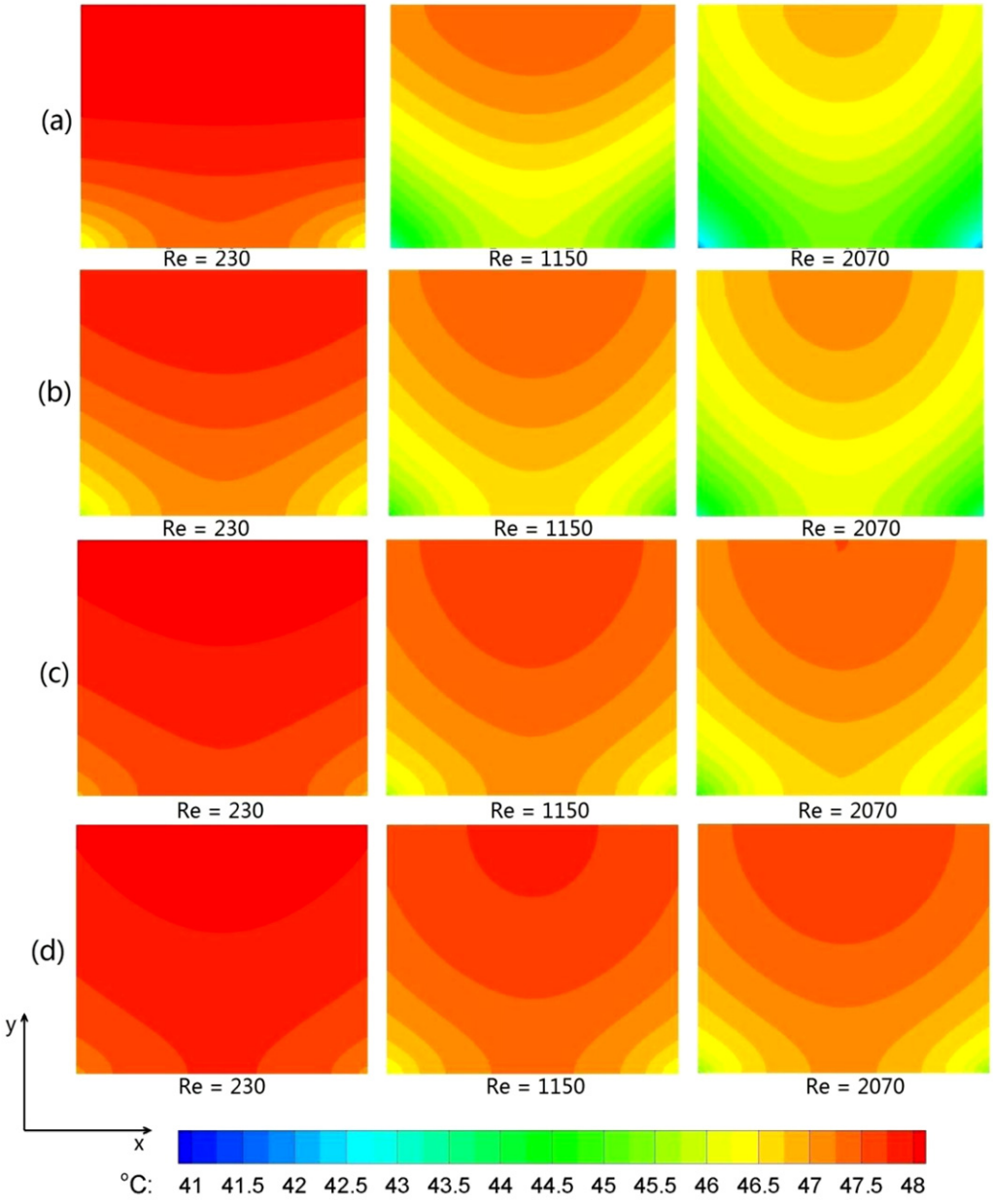

Fig. 14. Temperature distributions in the flat-plate battery stacks with different channel sizes and inlet Reynolds numbers at the end of the discharging processes. (a) channel size = 2 mm, $\alpha = 0.014$; (b) channel size = 4 mm, $\alpha = 0.027$; (c) channel size = 8 mm, $\alpha = 0.055$; (d) channel size = 12 mm, $\alpha = 0.082$.

to customize the formulation. For the two-dimensional computational domain of the flat-plate design, the mesh sizes are 0.25 mm per grid point and 0.5 mm per grid point in cooling channel along the *x*- and *y*-directions, respectively; and they are 0.9125 mm per grid point and 0.5 mm per grid point in battery units, as shown in Fig. 5. The mesh area of the three-dimensional model is 0.23 mm^2 in the cross-section of cooling channel and 0.31 mm^2 in battery unit, and the size along the *z*-direction is 6.5 mm per grid point, as shown in Fig. 6. Grid independent study has been carefully carried out to ensure that the change of results is negligible by further increasing the number of grid points. The convergence criterion is 1×10^{-8} for all the variables. The time step size is 1 s.

3. Analytical model

An analytical model is also developed for quick calculation of battery thermal behaviors. In addition, since the related experimental data are difficult to find in literature, the comparison between the numerical and analytical results may be considered as a piece of evidence for the rationality of the models. The schematic of the analytical model for the flat-plate battery stack is shown in Fig. 7, with a number of battery units connected in series. A symmetry boundary condition is considered on the right hand side of this figure. The boundary in contact with the cooling channel is considered as a convective heat transfer boundary condition, with the convective heat transfer coefficient and surrounding temperature being defined. The temperature and total heat generation rate of each battery unit are considered to be evenly distributed, and during a discharging process, each battery unit has a different volume averaged temperature and total heat generation rate, and the conductive heat transfer between the battery units is considered in this model.

For the battery unit in contact with the cooling channel, the energy balance can be represented as

$$\rho_b c_{pb} \Lambda (T_{1+\Delta t} - T_1) = hs\left(T_f - T_1\right)\Delta t + k_b s(T_2 - T) + S_{T1}\Lambda\Delta t \quad (19)$$

where Λ (m^3) is the volume of each battery unit, and s (m^2) is the area of battery surface. T_1 (°C) is the volume averaged temperature of the battery unit (named as battery unit 1) at the time instance t (s), $T_{1+\Delta t}$ (°C) is the volume averaged temperature of the battery unit at the time instance of $(t + \Delta t)$ (s), and h (W m^{-2} °C) is the convective heat transfer coefficient, which can be calculated as [19]

$$h = \frac{Nuk_a}{L} \quad (20)$$

where Nu is the Nusselt number, k_a (W m^{-1} K^{-1}) is the thermal conductivity of air, and L (m) is the length along the cooling channel. Depending on the cooling channel designs, fluid properties and flow velocities, different empirical correlations (for example, the related empirical correlations can be found in Ref. [19]) can be used to calculate Nu and h. Therefore, the effect of Reynolds number (indicated by the flow velocity and channel design) of cooling air on the battery thermal behaviors can be investigated by using this model.

For the other battery units (named as battery unit i), the energy balance can be represented as

$$\rho_b c_{pb} \Lambda (T_{i+\Delta t} - T_i) = k_b s(T_{i-1} + T_{i+1} - 2T) + S_{Ti}\Lambda\Delta t \quad (21)$$

The rest of the formulation related to the material properties and heat generations is described in Section 2. Therefore, with the initial conditions being set, the temperatures in the battery units at different time instances can be calculated one by one. The time step size is 1 s, and the time step size independent study has been carefully carried out to ensure that the change of results is negligible by further decreasing the time step size.

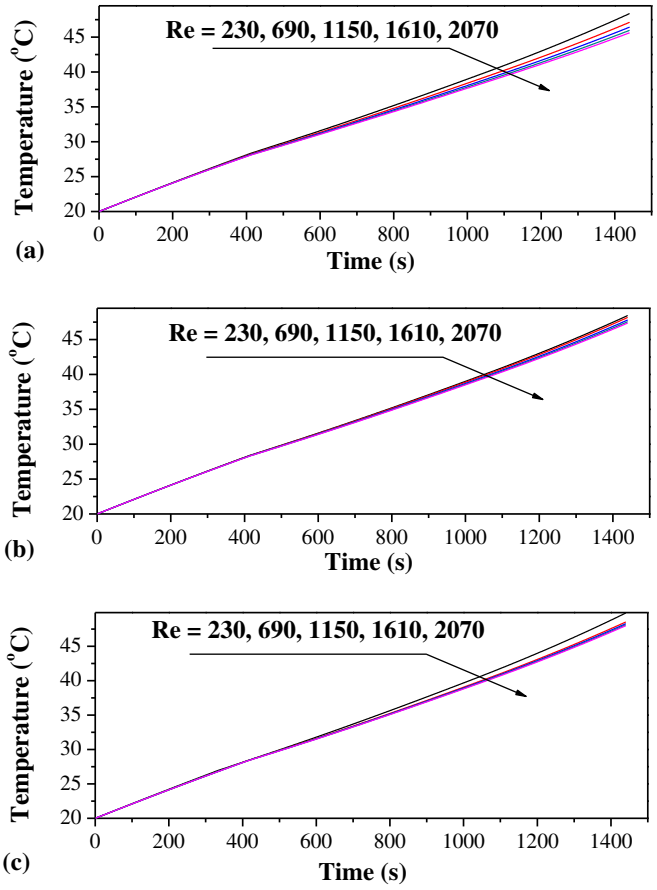

Fig. 15. Evolutions of volume averaged temperatures of the flat-plate battery stacks with different battery unit numbers per 4 mm cooling channel and inlet Reynolds numbers during the discharging processes. (a) 10 battery units per cooling channel, $\alpha = 0.055$; (b) 20 battery units per cooling channel, $\alpha = 0.027$; (c) 30 battery units per cooling channel, $\alpha = 0.018$.

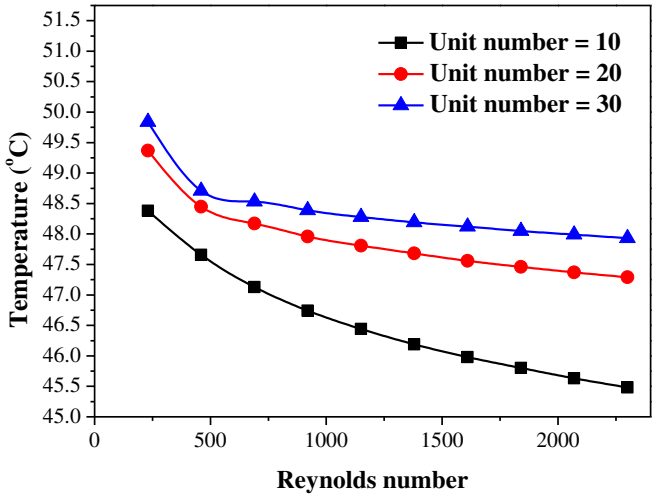

Fig. 16. Volume averaged temperatures of the flat-plate battery stacks with an inlet Reynolds number of 1150 and different battery unit numbers per 4 mm cooling channel at the end of the discharging processes (10 battery units per cooling channel, $\alpha = 0.055$; 20 battery units per cooling channel, $\alpha = 0.027$; 30 battery units per cooling channel, $\alpha = 0.018$).

4. Results and discussion

In the following subsections, the results of the numerical and analytical models are compared first. Since the numerical model is multi-dimensional and can consider more detailed design and operating conditions than the analytical model, most of the results presented in this study are obtained from the numerical model. The effect of cooling channel size and number of cooling channel on the thermal behavior of both the flat-plate and cylindrical battery stacks are investigated in details. The stack configurations and operating conditions are given in Tables 3 and 5. The initial battery stack temperature and the supplied cooling air temperature are set to be the same as the ambient temperature (20 °C). The ratio between the volume of the cooling channel and the volume of the battery is defined as a dimensionless parameter, α, as stated above. α therefore represents the compactness of the battery stacks. The ratio between the heat taken away by the cooling air from the battery and the power consumption for supplying coolant is another dimensionless parameter, β. β therefore can be considered as an energy efficiency factor of the cooling channel design.

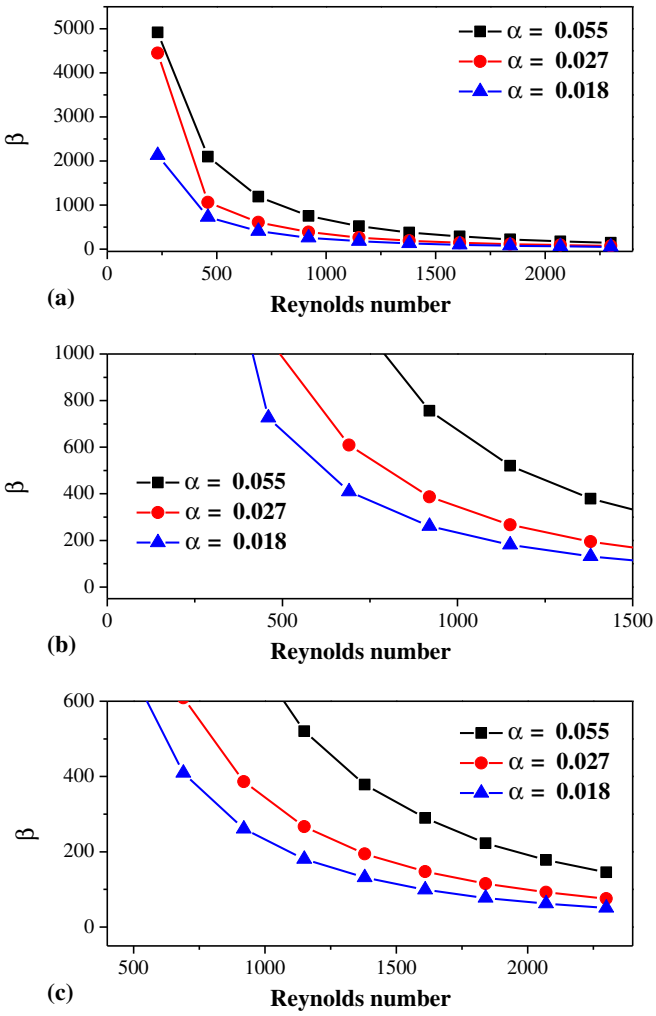

Fig. 17. Cooling efficiency factors (β) of the flat-plate battery stacks with different battery unit numbers per 4 mm cooling channel (α) and inlet Reynolds numbers of cooling air for the discharging processes (10 battery units per cooling channel, $\alpha = 0.055$; 20 battery units per cooling channel, $\alpha = 0.027$; 30 battery units per cooling channel, $\alpha = 0.018$).

4.1. Comparison between numerical and analytical results

The evolution of volume averaged temperature of a flat-plate battery stack during the discharging process obtained from the numerical and analytical models are shown in Fig. 8. The cooling channel size in the numerical model is 4 mm with an inlet Reynolds number of 1610 for the cooling air. The average convective heat transfer coefficient on the battery surface contacting the cooling channel in the analytical model is 20 W m^{-2} °C. The other parameters in these two models are the same. It can be seen from the Fig. 8 that the results of the numerical and analytical models agree reasonably. Since the related experimental data are difficult to find in literature, this comparison may be considered as a piece of evidence for the rationality of the models. In the following subsections, most of the results presented are from the numerical model because more detailed design and operating conditions can be considered.

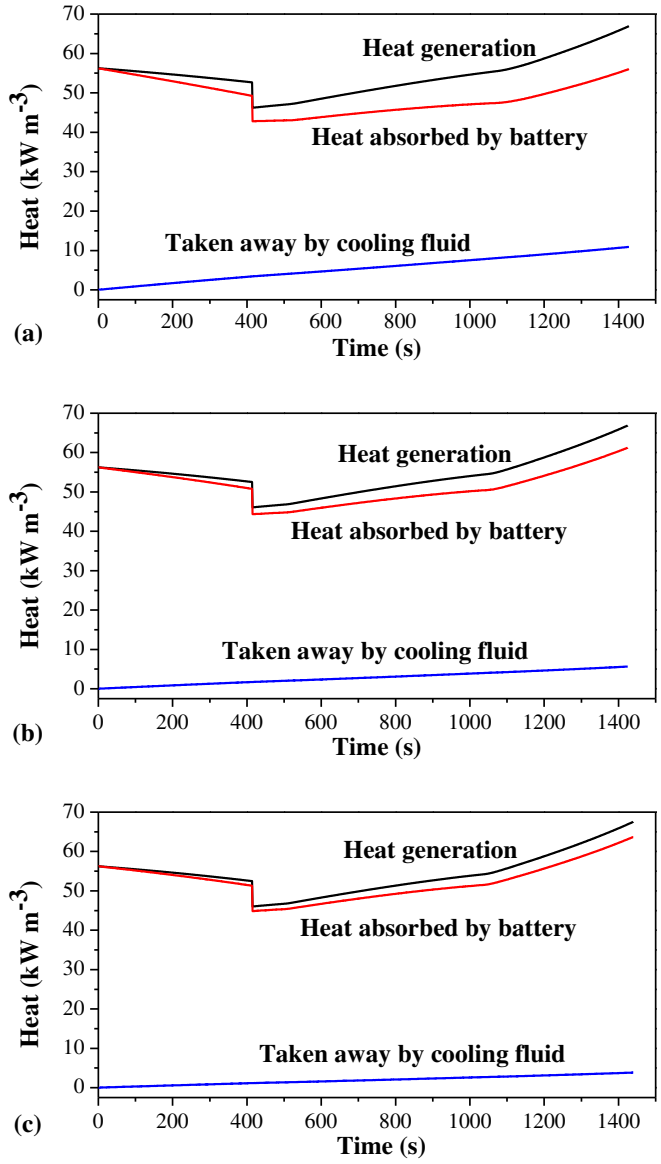

Fig. 18. Rates of heat generation, heat absorbed by battery and heat taken away by cooling air for the flat-plate battery stacks with an inlet Reynolds number of 1150 and different battery unit numbers per 4 mm cooling channel during the discharging processes. (a) 10 battery units per cooling channel, $\alpha = 0.055$; (b) 20 battery units per cooling channel, $\alpha = 0.027$; (c) 30 battery units per cooling channel, $\alpha = 0.018$.

4.2. Effect of cooling channel size of the flat-plate battery stacks

Fig. 9 shows the evolutions of volume averaged temperatures during the discharging processes with different cooling channel sizes and inlet Reynolds numbers for the flat-plate design. It can be noticed that the temperature differences with different inlet Reynolds numbers increase during the discharging processes. With a smaller cooling channel, the effect of inlet Reynolds number becomes more significant. Since the highest temperatures are reached at the end of the discharging processes, Fig. 10 shows the temperature distribution in the flat-plate battery stack with a cooling channel size of 4 mm at the end of the discharging processes with different inlet Reynolds numbers. The highest temperature appears in the middle between the cooling channels. With the lowest inlet Reynolds number of 230, the highest temperature of 48.89 °C is achieved in the middle, and it is 45.91 °C with the highest inlet Reynolds number of 2300. The cooling effect is more significant in the units close to the cooling channel on both sides. The temperature is more evenly distributed in the battery stack with a lower inlet Reynolds number.

The volume averaged temperatures of the battery stacks with different cooling channel sizes and inlet Reynolds numbers at the end of the discharging processes are shown in Fig. 11. With a larger cooling channel, the equivalent diameter of the channel is larger, resulting in a lower flow velocity in the channel with the same inlet Reynolds number. The temperature difference with the different cooling channel sizes at low inlet Reynolds numbers is insignificant, and it becomes more noticeable at higher inlet Reynolds numbers. With the same inlet Reynolds numbers, a smaller channel also results in a better cooling effect in most cases, however, a smaller channel size may also results in a higher flow resistance.

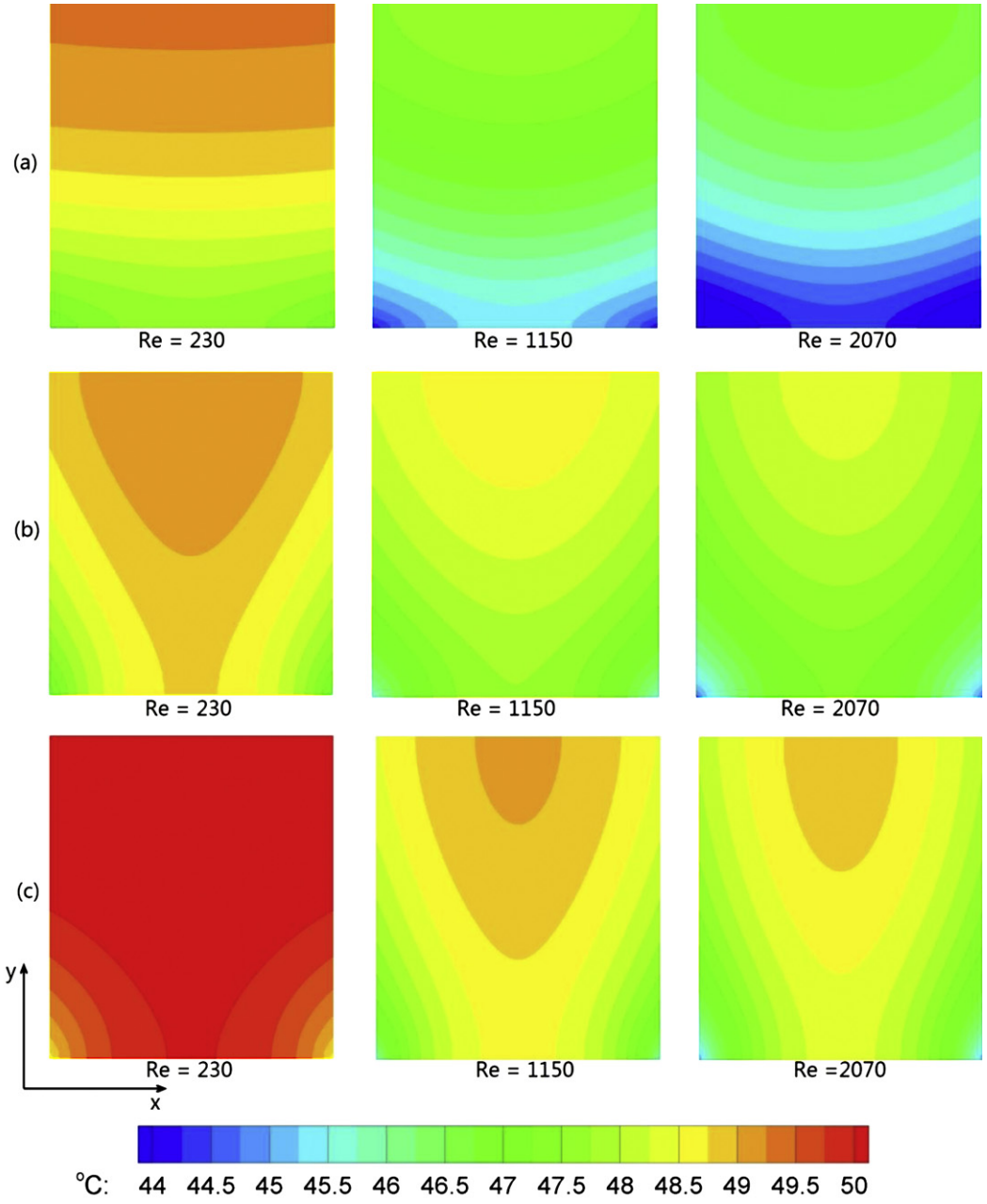

Fig. 19. Temperature distributions in the flat-plate battery stacks with different battery unit numbers per 4 mm cooling channel and inlet Reynolds numbers at the end of the discharging processes. (a) 10 battery units per cooling channel, $\alpha = 0.055$; (b) 20 battery units per cooling channel, $\alpha = 0.027$; (c) 30 battery units per cooling channel, $\alpha = 0.018$.

As shown in Equations (1) and (2), α represents the compactness of a battery stack, and β can be considered as a cooling efficiency factor. A smaller α indicates that the stack is more compact, and a larger β means that the cooling effect is more energy-efficient. Fig. 12 shows the change of β with the inlet Reynolds number at different values of α for the discharging processes. At low inlet Reynolds numbers, the difference in cooling efficiency factors (β) with different cooling channel sizes (α) is very high (about 10^5). β is still around 100 for the smallest α (0.014) at the lowest inlet Reynolds number (230). A value of 100 for β is still acceptable according to Equation (2). However, at higher inlet Reynolds numbers, for example, at 2300, the value of β becomes around 7, which may not be suitable in terms of the energy efficiency. On the other hand, the values of β are all fairly high with larger cooling channels ($\alpha \geq 0.027$). It can also be observed that the efficiency factor (β) always decreases with the inlet Reynolds number. Moreover, even though a low inlet Reynolds number may ensure acceptable energy efficiency, the cooling effect still needs to be considered. The results suggest that the cooling channel size needs to be large enough to maintain the cooling energy efficiency at different cooling air flow rates, and the volume ratio of cooling channel to battery needs to be higher than 0.014 when the inlet Reynolds number of cooling air is around 2000 or higher with a high discharging rate of 2 C. In addition, it is suggested that further increasing the cooling air flow rate (i.e. turbulent flow) may result in low energy efficiency for the thermal management of lithium ion battery stacks.

The rates of heat generation, heat absorbed by battery and heat taken away by cooling air for the flat-plate battery stacks with different cooling channel sizes and an inlet Reynolds number of cooling air of 1150 during the discharging processes are shown in Fig. 13. The heat generation includes three parts, which are from the electrochemical reactions (reaction heat), transport of electrons and ions (ohmic heat) and change of entropy (reversible heat). It can be noticed that at the same inlet Reynolds number, the cooling effect is stronger with a smaller cooling channel size (more heat can be taken by the cooling air). The rate of heat removal is increased during the discharging processes because the battery temperature is increased, leading to stronger heat transfer. There is a sudden drop of the heat generation and absorption rates during the discharging processes, mainly caused by the change of the reversible heat (change of entropy) according to Equation (13). The heat generation rate generally follows a decreasing trend, a sudden drop after that, and then an increasing trend, and the heat absorption rate follows the same trend as the heat generation rate.

Fig. 14 shows the temperature distributions in the flat-plate battery stacks with different channel sizes and inlet Reynolds numbers at the end of the discharging processes. It can be noticed that the temperature is higher but more evenly distributed with a lower inlet Reynolds number and a higher cooling channel size. The lowest temperature always appears on the sides of the batteries close to the cooling channel inlets, and the highest temperature is in the middle of the batteries close to the cooling channel outlets. The maximum temperature difference is about 5 °C in Fig. 14. In order to achieve better cooling effect and more evenly distributed temperature, the results in this figure suggest that a counter-flow arrangement of the cooling channels or changing the flow direction of the co-flow arrangement periodically may improve the thermal management effect. However, these designs may increase the manufacturing and operating complexity and cost.

4.3. Effect of number of cooling channels of the flat-plate battery stacks

The evolutions of volume averaged temperatures for the flat-plate battery stacks during the discharging processes with

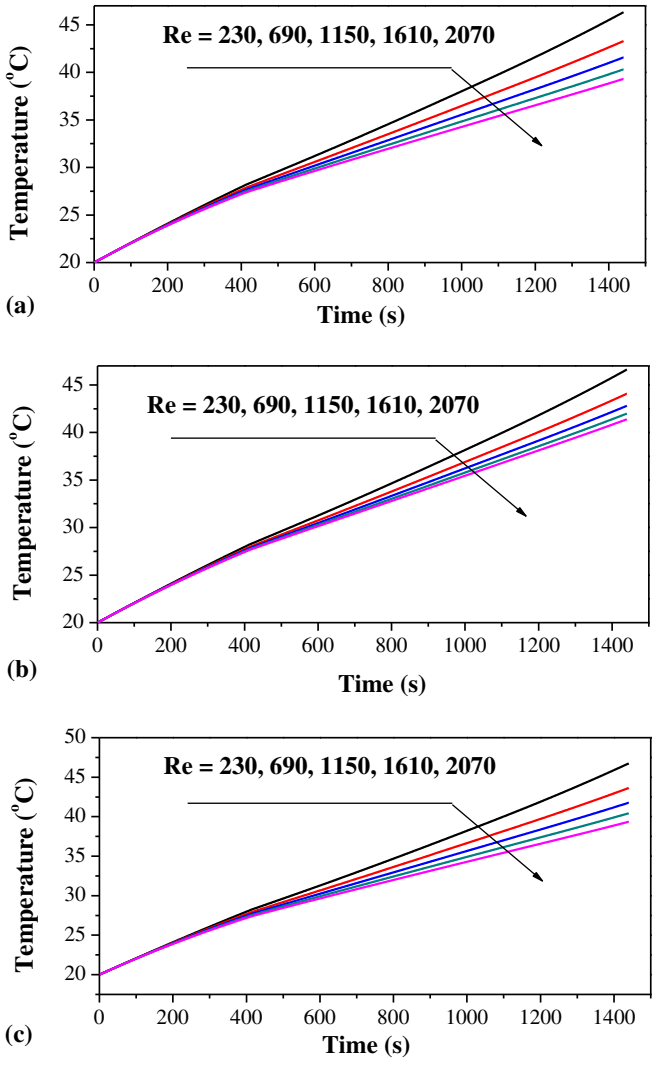

Fig. 20. Evolutions of volume averaged temperatures of the cylindrical battery with different cooling channel sizes and inlet Reynolds numbers of cooling air during the discharging processes. (a) $\alpha = 0.33$, distance between battery units = 0; (b) $\alpha = 0.90$, distance between battery units = 2 mm; (c) $\alpha = 2.54$, distance between battery units = 6 mm.

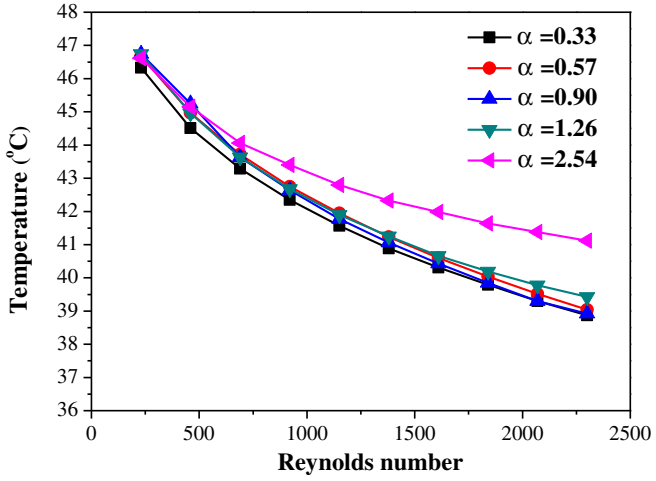

Fig. 21. Volume averaged temperatures of the cylindrical battery with different inlet Reynolds numbers of cooling air and cooling channel sizes at the end of the discharging processes.

different battery unit numbers (10, 20 and 30) per 4 mm cooling channel and different inlet Reynolds numbers are shown in Fig. 15, and similar to Fig. 9, the temperature differences with different inlet Reynolds numbers increase during the discharging processes. Fig. 16 shows the volume averaged temperatures of the flat-plate battery stacks with an inlet Reynolds number of 1150 and different battery unit numbers per 4 mm cooling channel at the end of the discharging processes. It can be noticed that with less battery units between two cooling channels, increasing the cooling air inlet Reynolds number has more significant cooling effects, and the improvement in the cooling effect becomes less significant at high inlet Reynolds numbers. With an inlet Reynolds number of 2300, for 20 battery units between 2 mm cooling channels (α = 0.014, Fig. 11) and 30 battery units between 4 mm cooling channels (α = 0.018, Fig. 16), the final temperatures are about 46.5 °C and 45.5 °C, respectively, indicating that a more compact battery stack is generally heated more significantly during a discharging process. For the same compactness (α = 0.055) but with different stack configurations (20 battery units between 8 mm cooling channels in Figs. 10 and 11 battery units between 4 mm cooling channels in Fig. 16), the final temperatures are all about 47.9 °C with an inlet Reynolds number of 2300. The results in Figs. 11 and 16 suggest that changing the cooling channel size and the number of cooling channels results in similar volume averaged temperatures for lithium ion battery stacks. However, the cooling channel size may affect the flow resistance of cooling air, and the number of battery units between cooling channels may have different temperature distributions, which need to be further investigated.

The cooling efficiency factors (β) of the flat-plate battery stacks with different battery unit numbers per 4 mm cooling channel (α) and inlet Reynolds numbers of cooling air for the discharging processes are shown in Fig. 17. It can be noticed that the general

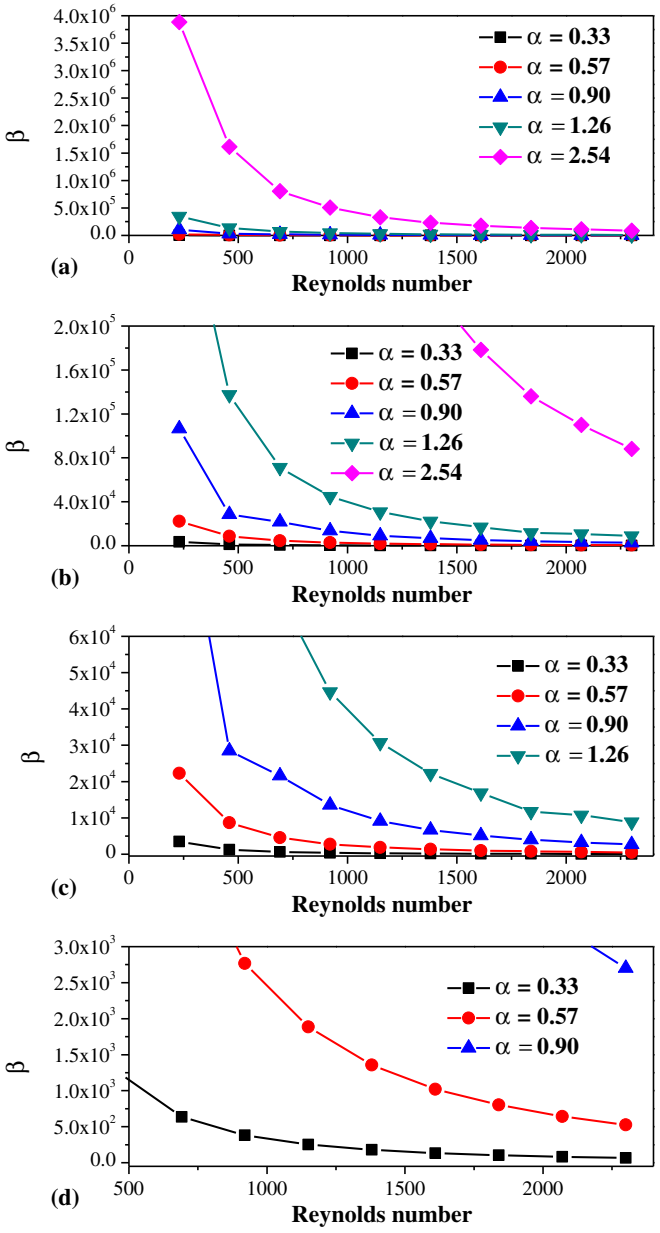

Fig. 22. Cooling efficiency factors (β) of the cylindrical battery stacks with different channel sizes (α) and inlet Reynolds numbers of cooling air for the discharging processes.

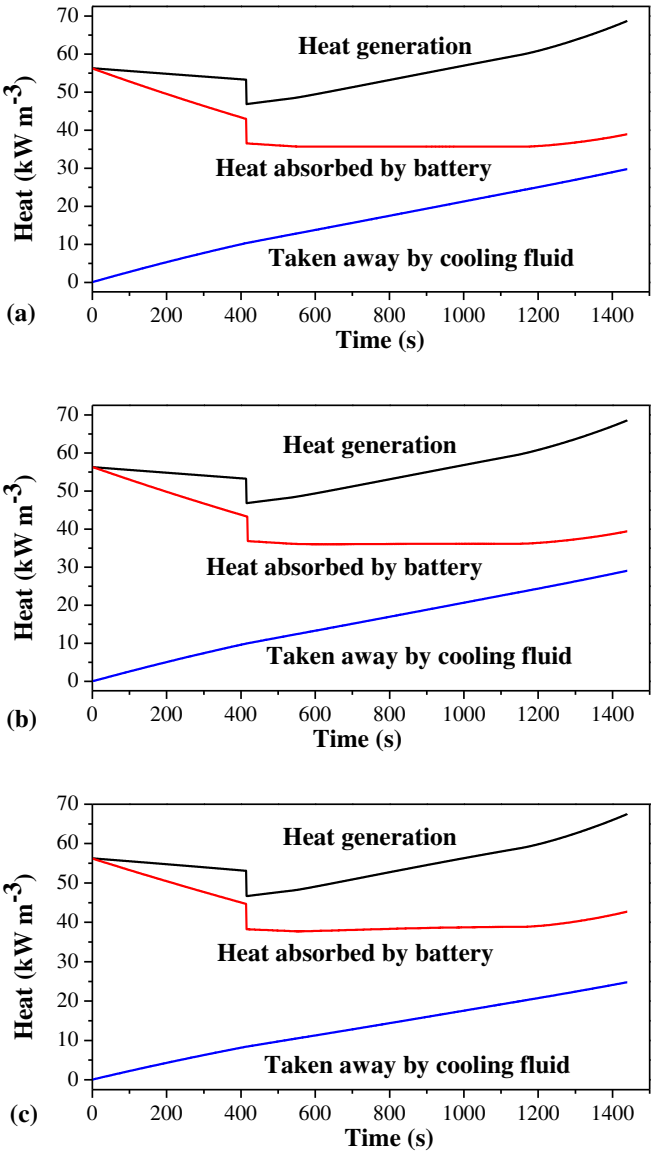

Fig. 23. Rates of heat generation, heat absorbed by battery and heat taken away by cooling air for the cylindrical battery stacks with an inlet Reynolds number of 1150 and different cooling channel sizes during the discharging processes. (a) α = 0.33, distance between battery units = 0; (b) α = 0.90, distance between battery units = 2 mm; (c) α = 2.54, distance between battery units = 6 mm.

trends are similar to Fig. 12 with different cooling channel sizes. However, with an inlet Reynolds number of 2300, for the same compactness ($\alpha = 0.055$) but with different stack configurations (20 battery units between 8 mm cooling channels in Figs. 10 and 12 battery units between 4 mm cooling channels in Fig. 17), the cooling energy efficiency factors (β) are about 600 and 150, indicating that a larger cooling channel improves the cooling energy efficiency. The results in Figs. 12 and 17 suggest that for the same compactness of battery stacks, increasing the channel size (increasing the number of battery units between cooling channels) improves the energy efficiency. However, with more battery units between cooling channels, the temperature may become more unevenly distributed, which needs to be further investigated. In addition, the rates of heat generation, heat absorbed by battery and heat taken away by cooling air for the flat-plate battery stacks with an inlet Reynolds number of 1150 and different battery unit numbers per 4 mm cooling channel during the discharging processes are shown in Fig. 18, and it can be noticed that the general trends in Fig. 18 is similar to Fig. 13.

Fig. 19 shows the temperature distributions in the flat-plate battery stacks with different battery unit numbers per 4 mm cooling channel and inlet Reynolds numbers at the end of the discharging processes. It can be observed that for the same inlet Reynolds numbers, with more battery units between cooling channels, the temperature is more unevenly distributed. The results in Figs. 9–19 suggest that for the same compactness of battery stacks (same volume ratio of channel to battery unit), changing the cooling channel size and the number of cooling channels results in similar volume averaged temperatures of the battery units, however, increasing the cooling channel size improves the cooling energy efficiency but results in more unevenly distributed temperature in the battery units, and vice versa.

4.4. Effect of cooling channel size of the cylindrical battery stacks

For cylindrical battery stacks, Figs. 2, 4 and 6 show that the cooling channels are formed between the cylindrical battery units. The smallest cooling channel is formed when the distance between the battery units is 0, as listed in Table 3, and the cylindrical battery stacks are generally less compact than the flat-plate battery stacks.

The evolutions of volume averaged temperatures of the cylindrical battery stacks with different cooling channel sizes and inlet Reynolds numbers of cooling air during the discharging processes are shown in Fig. 20, and similar to the flat-plate stacks in Figs. 9 and 15, the temperature differences with different inlet Reynolds numbers increase during the discharging processes. At the end of the discharging processes, as shown in Fig. 21, at low inlet Reynolds numbers, the final average temperatures are similar; and at high inlet Reynolds numbers, the differences in the average temperatures become significant, and with the same inlet Reynolds number, a more compact stack has a lower average temperature.

The energy efficiency factor (β) for the cylindrical stacks with different cooling channel sizes and inlet Reynolds numbers of cooling air are shown in Fig. 22. It can be noticed that the lowest energy efficiency factor (β) with the most compact design ($\alpha = 0.33$ and the distance between battery units is 0) and the highest Reynolds number of 2300 is still about 50, which is still an acceptable value according to Equation (2). The energy efficiency for the cylindrical stacks is generally higher than the flat-plate stacks, because the cooling channels in the cylindrical stacks considered in this study are generally larger (less compact) than the flat-plate stacks (Table 3). Perhaps further increasing the diameter of the cylindrical battery units can improve the compactness.

Corresponding to Figs. 13 and 18 of the flat-plate stacks, the rates of heat generation, heat absorbed by battery and heat taken away by cooling air for the cylindrical battery stacks with an inlet Reynolds number of 1150 and different cooling channel sizes during the discharging processes are shown in Fig. 23. It can be noticed that the general trends are similar in these figures. The temperature distributions in the cylindrical battery stacks with different channel sizes and inlet Reynolds numbers at the end of the discharging processes are shown in Fig. 24. The temperature distributions are generally similar, following a decreasing trend along the cooling air flow direction. It can also be noticed that a larger cooling channel size results in a more even temperature distribution, and a higher inlet Reynolds number of cooling air enhances the cooling effect. The temperature distributions in this figure and Figs. 14 and 19

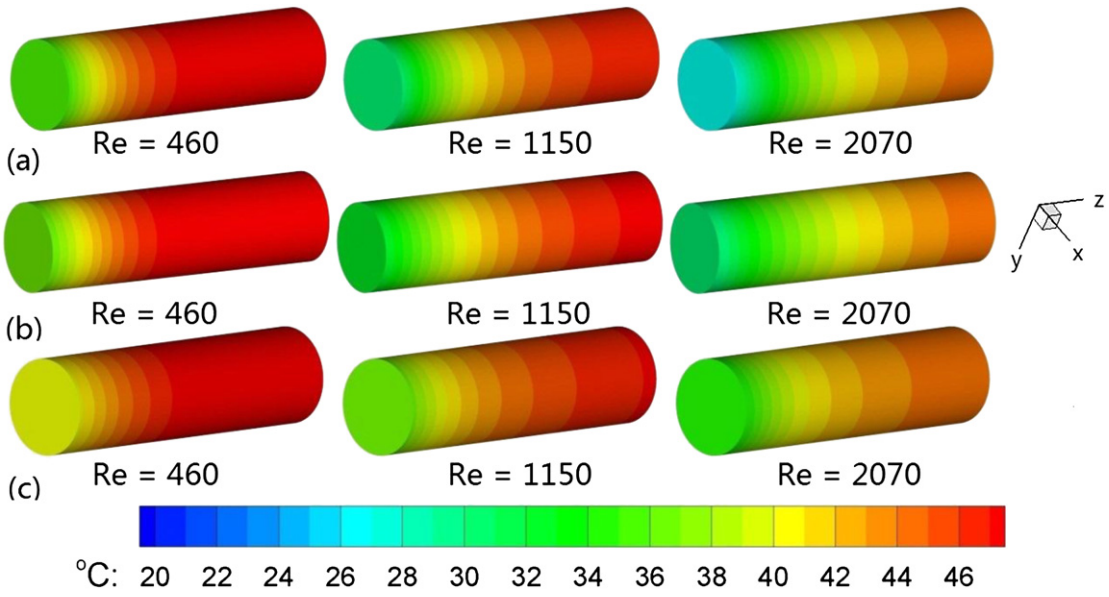

Fig. 24. Temperature distributions in the cylindrical battery stacks with different channel sizes and inlet Reynolds numbers at the end of the discharging processes. (a) $\alpha = 0.33$, distance between battery units = 0; (b) $\alpha = 0.90$, distance between battery units = 2 mm; (c) $\alpha = 2.54$, distance between battery units = 6 mm.

suggest that a counter-flow arrangement of the cooling channels or changing the flow direction of the co-flow arrangement periodically may improve the evenness of temperature distribution. However, as mentioned previously, these designs may increase the manufacturing and operating complexity and cost.

5. Conclusion

In this study, a multi-dimensional numerical model and an analytical model for the thermal management of lithium ion battery stacks have been developed to investigate the thermal behaviors of flat-plate and cylindrical battery stacks during discharging processes. A reasonable agreement between the results obtained from these two models has also been obtained. Two dimensionless parameters, α and β, representing the compactness and cooling energy efficiency of battery stacks are defined. It is found that for the same compactness of flat-plate battery stacks (same volume ratio of channel to battery unit), changing the cooling channel size and the number of cooling channels results in similar volume averaged temperatures of the stacks, however, increasing the cooling channel size improves the cooling energy efficiency but results in more unevenly distributed temperature in the battery units, and vice versa. It is suggested that the volume ratio of cooling channel to battery (α) needs to be higher than 0.014 when the inlet Reynolds number of cooling air is around 2000 or higher with a high discharging rate of 2 C. The cylindrical battery stacks considered in this study are generally less compact (α) and more energy-efficient (β) than the flat-plate battery stacks, and the general thermal behaviors are similar between these two designs. In order to achieve better cooling effect and more evenly distributed temperature, it is suggested that a counter-flow arrangement of the cooling channels or changing the flow direction of the co-flow arrangement periodically may improve the thermal management. However, these designs may increase the manufacturing and operating complexity and cost.

Acknowledgments

This research is supported by the National Natural Science Foundation of China (Grant Nos. 51276121 and 51206117) and the Natural Science Foundation of Tianjin (China) (Grant No. 12JCYBJC30500).

References

[1] L. Chen, K.Chen. and SunFengchun, 5th IEEE Vehicle Power and Propulsion Conference vol. 20, pp. 1643–1648.
[2] P. Moss, G. Au, E.J. Plichta, P. Zheng, Journal of Electrochemical Society 155 (2008) 986–994.
[3] J. Zhang, et al., IEEE Transactions on Energy Conversion 25 (2010) 1133–1141.
[4] H. Horie, T. Abe, T. Kinoshita, The Word Electric Vehicle Journal, 2 (2008) 25–30.
[5] K. Smith, G.H. Kim, E. Darcy, A.Pesaran, International Journal of Energy Research. Special issue: electrical energy storage for future transportation and renewable energy. (34) Issue 2, 204–215.
[6] C. Forgez, D.V. Do, G. Friedrich, M. Morcrette, C. Delacourt, Journal of Power Sources 195 (2010) 2961–2968.
[7] H. Maleki, A.K. Shamsuri, Journal of Power Sources 115 (2003) 131–136.
[8] S. Al Hallaj, J. Prakash, J.R. Slman, Journal of Power Sources 87 (2000) 186–194.
[9] A. Mills, S. Al-Hallaj, Journal of Power Sources 141 (2005) 307–315.
[10] R. Kizilel, A. Lateef, R. Sabbaha, M.M. Farid, J.R. Selman, S. Al-Hallaj, Journal of Power Sources 183 (2008) 370–375.
[11] X. Duan, G.F. Naterer, International Journal of Heat and Mass Transfer 53 (2010) 5176–5182.
[12] G. Karimi, X. Li, International Journal of Energy Research (2012). http://dx.doi.org/10.1002/er.1956.
[13] Y. Chen, J.W. Evans, Electrochemical Acta 39 (1994) 517–526.
[14] Y. Inui, et al., Energy Conversion and Management (2007) 2103–2109.
[15] W. Fang, O.J. Kwon, C.Y. Wang, International Journal of Energy Research 34 (2010) 107–115.
[16] R. Sabbah, R. Kizilel, J.R. Selman, S. Al-Hallaj, Journal of Power Sources 182 (2008) 630–638.
[17] R. Kizilel, R. Sabbah, J.R. Selman, S. AL-Hallaj, Journal of Power Sources 194 (2009) 1105–1112.
[18] Sony Co, SONY Battery Manual for SONYUS18650 (1993).
[19] Y.A. Cengel, Heat Transfer: A Practical Approach, second ed., McGraw-Hill, Boston, 2003.